

# Diffusion of H<sub>2</sub> and D<sub>2</sub> Confined in Single-Walled Carbon Nanotubes: Quantum Dynamics and Confinement Effects.

Manel Mondelo-Martell and Fermín Huarte-Larrañaga\*

*Department of Materials Science & Physical Chemistry and Institute of Theoretical and  
Computational Chemistry (IQTUB), Universitat de Barcelona, Barcelona*

E-mail: [fermin.huarte@ub.edu](mailto:fermin.huarte@ub.edu)

Phone: +34 93 4031341. Fax: +34 93 4021231

---

\*To whom correspondence should be addressed

## Abstract

We present quantum dynamics calculations of the diffusion constant of  $\text{H}_2$  and  $\text{D}_2$  along a single-walled carbon nanotube at temperatures between 50 and 150 K. We calculate the respective diffusion rates in the low pressure limit by adapting well-known approaches and methods from the chemical dynamics field using two different PES to model the C–H interaction. Our results predict a usual kinetic isotope effect, with  $\text{H}_2$  diffusing faster than  $\text{D}_2$  in the higher temperature range, but a reverse trend at temperatures below 50–70 K. These findings are consistent with experimental observation in similar systems, and can be explained by the different effective size of both isotopes resulting from their different ZPE.

## 1 Introduction

Nanostructured materials have received a lot of attention in the last years due to their unique properties in fields such as mechanics, electronics, fluidics and storage technologies.<sup>1–8</sup> In particular, their suitability as storage devices for small gaseous molecules has comprised a great deal of the research in the field due to its direct environmental impact. For instance, dangerous pollutants or greenhouse effect compounds can be kept off the atmosphere, or clean fuels such as hydrogen can be transported from production to consumption sites, thus spreading its use.<sup>1,9–16</sup> The study of these substrate-gas systems has led to the discovery of *quantum confinement effects*, distortions of the molecular structure arising from the encapsulation in cavities of the order of the nanometer.<sup>17</sup> These effects have opened a new field of research, which tries to understand them in order to design novel and better storage devices<sup>18–26</sup> and find new technological applications. These applications include isotopic separation of compounds, either by selective adsorption<sup>17,27</sup> or kinetic effects,<sup>28</sup> to nanoconfined tailored reactions.<sup>29–31</sup>

Among all relevant molecules studied in the field of nanomaterial-gas interactions, hydrogen and its isotopologues are the most studied since the seminal work of Dillon et al.<sup>14</sup>

The reason for this is twofold: first, the obvious economical interest of hydrogen, which is regarded as a potential fuel for the near future, much more efficient and environmentally sustainable than current fossil fuels. However, its low density makes its storage in conventional devices highly inefficient, and this has pushed the research towards the study of novel devices to make the storage and transport feasible (See Ref. 11 and references therein). Secondly, hydrogen stands as an interesting molecule itself due to its low mass, which makes quantum effects much more highly noticeable and important than in the case of heavier atoms. A specially interesting effect appearing when these molecules are confined in nanostructures is the so-called *quantum sieving*, a large difference in the adsorption properties of two isotopologues due to their different zero point energy (ZPE). This effect has been posited as a potential separation method between hydrogen and deuterium molecules.<sup>17,27</sup> Inspired by this discovery, several theoretical works have been performed studying the dynamics of a hydrogen molecule in different nanometric cavities such as carbon nanotubes,<sup>23</sup> zeolites<sup>32</sup> or metal-organic frameworks (MOFs),<sup>21,33</sup> most of them focusing on the study of a rigid molecule with motion confined to a single unit cell of the material. Some of the milestones in the field are the work of Beenakker et al.,<sup>17</sup> which first described the quantum sieving effect, and the work of Lu et al.<sup>23</sup> in which *extreme confinement* is presented. More recently, Bacic and coworkers have made important advances in this field through the use of modern potential energy surfaces to study new systems and compare their results with experimental data,<sup>20,21</sup> thus providing new evidence and explanations of the quantum confinement effects. However, only few works have considered so far the motion of the molecule along the periodic dimensions of the different nanomaterials at full quantum level, being the two most recent by Skouteris and Laganà<sup>34</sup> and ourselves.<sup>19</sup> The dynamics of the diffusion process are important to explain an additional effect, the *kinetic molecular sieving* predicted by Kumar and Bhatia<sup>35</sup> and experimentally confirmed by Nguyen et al.<sup>36</sup> and Contescu et al.,<sup>37</sup> which involves a faster diffusion of D<sub>2</sub> in front of H<sub>2</sub> when confined in certain nanostructured materials. This trend, which opposes the usual kinetic isotope effect, could improve

the separation of isotopologues. Although the quantum sieving effect on carbon nanotubes has been previously studied by several groups from a stationary point of view,<sup>23,38</sup> focusing on the selective adsorption of  $D_2$  in front of  $H_2$ , a simulation of the actual dynamics of the diffusion in these materials at a quantum level is still missing.

In the present work, we make our first attempt to compute diffusion rates of molecular hydrogen inside a carbon nanotube using quantum dynamics approaches. Although diffusion is known to be one of the processes most affected by quantum confinement effects, full quantum simulations in nanoconfined systems are still missing. On the other hand, diffusion has been theoretically studied on heterogeneous gas-surface systems for a long time, and diffusion rates have been calculated with quantum dynamics methods, which provides a solid theoretical ground for similar studies on nanostructures. These methods range from the development of specific master kinetic equations specific for diffusion processes<sup>39,40</sup> to the adaptation of chemical kinetics formalisms.<sup>41,42</sup> Thus, our work focuses on the rigorous quantum mechanical calculation of the diffusion rate constant for a single hydrogen or deuterium molecule inside an (8,0) single-walled carbon nanotube (SWCNT) through the adaptation of the work of Zhang et al., who successfully reproduced the experimental behavior of a single H atom on a copper surface using a fully quantum mechanical approach. In addition to this, the comparison of  $H_2$  and  $D_2$  diffusion rates inside carbon nanotubes could provide some additional insight on the sieving mechanism in other devices such as carbon molecular sieves.

The paper is structured as follows. In the first section the theoretical background of the study is described, including the approach used to calculate diffusion rates, an overview of the flux correlation function formalism and the calculation of partition functions. Also, a brief discussion on the model of the system and on the calculation method (the Multi-configurational Time-dependent Hartree method) is presented. Section 3 is devoted to the discussion of the actual results of the study, focusing on the computed diffusion coefficients. The selectivity factor for the isotopologues' adsorption is also calculated. Our results are

summarized in Section 4, where the main conclusions are drawn.

## 2 Theoretical Methods

### 2.1 Diffusion rate calculation

The process of the diffusion of a gas in a condensed phase, for low temperatures and low concentration of adsorbate, can be described by a *hopping model*<sup>43,44</sup>. In this model, the diffusion rate  $D(T)$  is considered to depend exclusively on the probability of a single molecule crossing from one binding site  $i$  to another binding site  $j$ :

$$D(T) = (1/2d) \sum_{j \neq i} k_{i \rightarrow j}(T) l_{ij}^2, \tag{1}$$

with  $k_{i \rightarrow j}$  the *hopping frequency* from site  $i$  to  $j$ ,  $l_{ij}$  the distance between binding sites, and  $d$  the symmetry number of the system. A parallelism between this model of diffusion and a chemical reaction can be established: in both cases we are concerned with the probability to go from a given thermal equilibrium configuration (*reactants*) to another (*products*), being both configurations separated by a potential energy barrier. There are nevertheless differences, one of them being that in diffusion one has several equivalent sites at different distances, while in a chemical reaction one is mainly concerned with one minimum of the potential energy surface (PES). However, as pointed out in Ref. 43, usually the most important hops occur between adjacent binding sites and Equation (1) can be simplified obtaining:

$$D(T) = (l^2/2d)k_{hop}(T). \tag{2}$$

The problem of diffusion is then reduced to the calculation of the hopping frequency between two adjacent binding sites,  $k_{hop}$ .

Several methods are found in the literature to compute  $k_{hop}$ , either classically or using

quantum mechanics. Within the classical mechanics framework, Molecular Dynamics (MD) and Grand Canonical Monte Carlo (GCMC) provide with methods for calculating either  $k_{hop}$  or even directly the diffusion rate via velocity correlation functions. Taking advantage of the similarities already outlined between chemical reactions and diffusion, other tools such as Transition State Theory (TST), can also be used. This latter approach implicitly implies two related approximations: the first one is the nearest neighbor approximation already discussed, and the other is the uncorrelated hopping approximation, which implies that once the substrate crosses the dividing surface it is directly considered as belonging to the product channel. This means, as it is well known, that the TST hopping frequency is an upper bound to the real  $k_{hop}$ , since no recrossing is allowed. On the other hand, specific models have been proposed to find  $k_{hop}$  in the quantum dynamics formalism (see Ref. 43 and references therein). In the present work we follow the work of Light and coworkers,<sup>41</sup> in which they calculated the hopping frequency using the Transition State Wave Packet method.<sup>45</sup> This approach is based on the use of the flux correlation function formalism first introduced by Miller.<sup>46</sup> Even though we will use the same basic concepts, our calculation of  $k_{hop}$  will rely on the calculation and propagation of the thermal flux operator eigenstates.

## 2.2 Description of the system

The model proposed for describing the diffusion of the hydrogen (or deuterium) molecule along a nanotube consists on a full dimensional representation of a single diatomic molecule, confined in the hollow cavity of a rigid (8,0) carbon nanotube made up from the concatenation of 20 unit cells in order to be able to disregard edge effects. The unit cell's geometry was obtained from a CRYSTAL09<sup>47</sup> optimization using the B3LYP functional and a 6-21G basis set in a periodic model, obtaining a unit cell length and diameter of 8.07 and 12.08 bohrs, respectively. Although the interaction between the structure phonons and the diffusion is known to be an important factor in diffusion,<sup>43,44</sup> we consider that the frozen structure model is a reasonable assumption for a first approach to the problem.

The system's Hamiltonian is therefore a 6D operator with the form:

$$\hat{H}_{6D} = -\frac{\hbar^2}{2\mu_{H_2}} \left( \frac{\partial^2}{\partial \rho^2} + \frac{2}{\rho} \frac{\partial}{\partial \rho} + \frac{1}{\rho^2} \frac{\partial^2}{\partial \theta^2} + \frac{1}{\rho^2} \frac{1}{\sin^2 \theta} \frac{\partial^2}{\partial \phi^2} \right) - \frac{\hbar^2}{2m_{H_2}} \left( \frac{\partial^2}{\partial x^2} + \frac{\partial^2}{\partial y^2} + \frac{\partial^2}{\partial z^2} \right) + \hat{V}(\rho, \theta, \phi, x, y), \quad (3)$$

where  $\rho$  stands for the internuclear distance between the atoms in the diatomic molecule,  $\theta$  and  $\phi$  represent respectively the polar and azimuthal angles of the molecular axis with respect to the nanotube's axis, and  $x$ ,  $y$ , and  $z$  are the coordinates of the center of mass of the molecule, being  $z$  coincident with the nanotube's axis. The 6D PES is given by a sum of Lennard-Jones pair interaction terms between the carbon and the hydrogen (or deuterium) atoms to represent the dispersion forces, and a Morse potential to take into account the covalent bond in the molecule:

$$\hat{V}_{6D} = V_{H-H}(\rho) + V_{C-H}(\rho, \theta, \phi, x, y, z), \quad (4)$$

$$\hat{V}_{C-H}(\rho, \theta, \phi, x, y, z) = \sum_{i=1}^2 \sum_{j=1}^{NC} V_{i,j}^{LJ}(d_{H_i-C_j}). \quad (5)$$

The parameters used to model the covalent interaction are well known ( $D_e = 0.1746$  hartree,  $a = 1.0271$  bohr<sup>-1</sup> and  $R_e = 1.4$  bohrs). Instead, several sets of Lennard-Jones parameters have been used in the past to model the C-H interactions in a nanotube. Among the available Lennard-Jones parameters, we have first selected a set used by us in our recent work,<sup>18,22,48</sup> with  $\sigma = 2.82$  Å and  $\epsilon = 0.0605$  kcal/mol (this potential will be referenced as Ref. 48 PES). Additionally, motivated by the large differences between the different potentials reported by Garberoglio et al.,<sup>38</sup> we have also used a second potential for our calculations. We have chosen the Frankland-Brenner potential, with  $\sigma = 3.08$  Å and  $\epsilon = 0.0549$  kcal/mol (FB PES). This potential was employed in Refs 23 and 38, predicting a remarkable quantum sieving.

Relaxed projections of the two potential energy surfaces used in the present work are

shown in Figure 1. The FB PES presents a tighter profile on the  $x$  dimension, which is consistent with the higher barriers for both rotation ( $\theta$ ) and diffusion ( $z$ ). This feature suggests a slower diffusion when using the FB PES rather than the Ref. 48 PES. Note, however, the energy scale of the potential energy cut along the  $z$  coordinate, which is of the order of few meV.

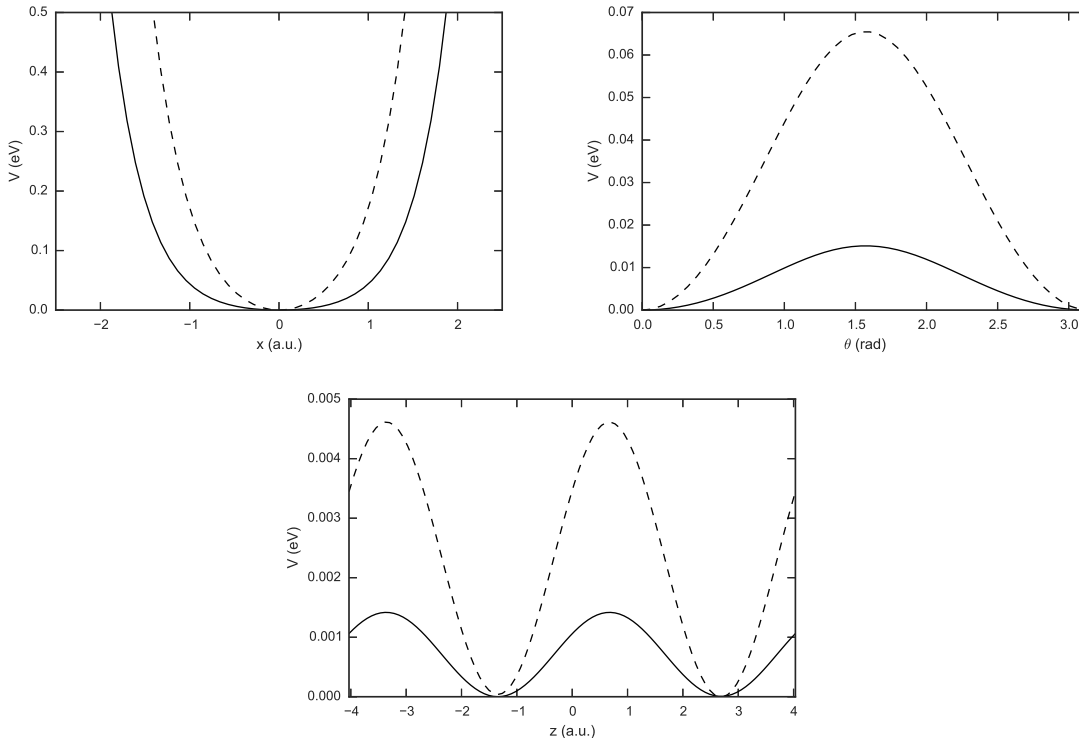


Figure 1: Relaxed projection of the Ref. 48 (solid) and FB (dashed) potential energy surfaces along the  $x$  (top-left),  $\theta$  (top-right) and  $z$  (bottom) DOFs.

### 2.3 Flux correlation functions and direct rate constant calculation

The methodology used to calculate the hopping frequency in the present work is explained in the present section. Note that atomic units are assumed throughout this section. For a complete discussion on the method in the context of chemical reactions, the reader is referred to Ref. 49.

The general expression for a reaction rate is given as a Boltzmann thermal average of its

cumulative reaction probability (CRP),  $N(E)$ :

$$k(T) = \frac{1}{2\pi Q_r(T)} \int_{-\infty}^{\infty} dE e^{-E\beta} N(E), \quad (6)$$

with  $\beta = 1/k_B T$ . The calculation of this quantity through *direct dynamics* methods is based on the correlation function formalism introduced by Miller and coworkers.<sup>46,50</sup> In the present work we use the approach by Matzkies and Manthe,<sup>51,52</sup> where the cumulative reaction probability is obtained as:

$$N(E) = \frac{1}{2} e^{\beta E} \sum_{f_{T_0}} f_{T_0} \int_{-\infty}^{\infty} dt \int_{-\infty}^{\infty} dt' e^{iEt} e^{-iEt'} \langle f_{T_0} | e^{i\hat{H}t'} \hat{F} e^{-i\hat{H}t} | f_{T_0} \rangle, \quad (7)$$

or, alternatively, as:

$$N(E) = \frac{1}{2} e^{\beta E} \sum_{f_{T_0/2}} \sum_{f'_{T_0/2}} f_{T_0} f'_{T_0} \left| \int_{-\infty}^{\infty} dt e^{iEt} \langle f_{T_0/2} | e^{i\hat{H}t} | f'_{T_0/2} \rangle \right|^2. \quad (8)$$

In Eqs (7) and (8),  $f_{T_0}$  and  $|f_{T_0}\rangle$  stand respectively for the eigenvalues and eigenstates of the *thermal flux operator*,  $\hat{F}_{T_0} = e^{-\beta\hat{H}} \hat{F} e^{-\beta\hat{H}}$ , and  $\hat{F}$  is in turn the *flux operator*, defined as:

$$\hat{F} = i \left[ h, \hat{H} \right], \quad (9)$$

where  $\hat{H}$  is the system's Hamiltonian, and  $h$  is a Heaviside function which separates reactants from products. Note that in Eq (8) the reference temperature of the thermal flux operator is divided by a factor of two. This equation may be used when the same flux operator is employed to obtain the flux eigenstates and analyze their propagation and it implies that, for a value of  $\beta = 1/kT_0$  we obtain information for temperatures equivalent to  $T_0/2$ . Regarding the Heaviside function, since we do not have a real chemical reaction but a diffusion process, the dividing surface is placed at a value of the diffusion coordinate corresponding to a saddle point of the PES separating two neighbor unit cells. Hence, we arbitrarily define the

geometries at one side of this dividing surface as *reactants*, and the remaining as *products*. Then, in order to take into account diffusion on both directions, we must multiply  $k(T)$  by a factor of two in order to obtain the hopping frequency  $k_{hop}$ .

Equation (9) can be rewritten in terms of the *flux-flux correlation function*,  $C_{ff}(t, t') = \sum_{f_{T_0}} f_{T_0} \langle f_{T_0} | e^{i\hat{H}t'} \hat{F} e^{-i\hat{H}t} | f_{T_0} \rangle$ :

$$N(E) = \frac{1}{2} e^{\beta E} \int_{-\infty}^{\infty} dt \int_{-\infty}^{\infty} dt' e^{iEt} e^{iEt'} C_{ff}(t, t') \quad (10)$$

This quantity and its time integral, the *flux-position correlation function*,  $C_{fp}$ , are central since their shape and limits can be used as convergence criteria for the computation of  $N(E)$ . In our case, the following scheme has been used to compute a hopping frequency for a diffusion problem:

1. Set a dividing surface at a maximum of the PES along the diffusing coordinate (the nanotube's axis).
2. Calculate the eigenstates of the thermal flux operator on this dividing surface at a given reference temperature,  $|f_{T_0}\rangle$ .
3. Propagate the eigenstates and Fourier transform the matrix elements of the flux operator to obtain the CRP. In this step, each flux eigenstate contribution is weighted by its corresponding degeneracy number depending on its rotational parity and whether it is D<sub>2</sub> or H<sub>2</sub>.
4. Obtain the hopping frequency by thermal averaging of  $N(E)$ .

In the present work all these steps are carried out using the State-Averaged Multiconfigurational Time-dependent Hartree (SA-MCTDH) method by Manthe<sup>53</sup> using the Bielefeld MCTDH software package, which is briefly discussed in Section 2.5.

## 2.4 Partition function calculation

Once the CRP is obtained, according to Equation (6), the second term needed to calculate a rate constant is the reactant partition function,  $Q(T)$ . In order to compute this term we have relied on the assumption of separability of this system<sup>19</sup> into a 1D *diffusing* degree of freedom (DOF) and a set of five *confined* DOFs:

$$Q(T) = q_{dif}(T)q_{con}(T). \quad (11)$$

The diffusing term in Eq (11) is then evaluated following the standard quasiclassical approximation for translational motion:

$$q_{dif} = \left( \frac{2\pi m k_B T}{h^2} \right)^{\frac{1}{2}} L, \quad (12)$$

where  $L$  is the length of the unit cell of the nanotube.

The calculation of the  $q_{con}(T)$  can be carried out either with a semiclassical or a fully quantum approach. Even though the semiclassical approximation is usually considered accurate enough for diatomic molecules, either free or adsorbed on surfaces, for a confined system it is not clear whether this model is reliable enough. For instance, the model relies on the full separability of all the DOFs, which is known to be too harsh an assumption on nanoconfined systems.<sup>18,22,23</sup> For this reason,  $q_{con}$  is actually calculated as the trace of the Boltzmann operator of the *confined* 5D Hamiltonian,  $\hat{H}_{con}(\rho, \theta, \phi, x, y)$ . This operator is equivalent to the one in Eq (3) but fixing the position along  $z$  at a -1.36 bohr, corresponding to an energy minimum. In order to take into account the total symmetry of the system with respect to particle exchange, the eigenstates of  $\hat{H}_{con}$  are classified according to their rotational parity and multiplied by the corresponding degeneracy number:

$$q_{conf} = g_e \sum_{\forall n} e^{-\beta E_n^e} + g_o \sum_{\forall n} e^{-\beta E_n^o}, \quad (13)$$

where  $E_n^e$  and  $E_n^o$  stand respectively for the energies of the eigenstates with even and odd parity with respect to rotation, placing the energy origin at the bottom of the PES. As it is discussed in the Results section, a comparison between the semiclassical and quantum partition functions reveals a difference of several orders of magnitude, so the use of the latter is fully justified in the present context.

## 2.5 MCTDH

As mentioned above, the SA-MCTDH method has been employed in the thermal flux eigenstate calculation and corresponding time propagation. In the standard MCTDH method,<sup>54</sup> a single wave function is represented as a sum of configurations *Ansatz* with the form:

$$\Psi(Q_1, \dots, Q_p, t) = \sum_{j_1=1}^{n_1} \cdots \sum_{j_p=1}^{n_p} A_{j_1 \dots j_p}(t) \prod_{k=1}^p \varphi_{j_k}^{(k)}(Q_k, t), \quad (14)$$

where each degree of freedom (DOF)  $k$  is represented by a set of low dimensional time-dependent basis functions  $\varphi_{j_k}^{(k)}$  known as Single Particle Functions (SPFs). These SPFs are in turn represented on a time-independent (*primitive*) basis set, usually consisting on DVR or FFT grids, thus giving rise to the *two layer representation* of the total wave function, which is behind the outstanding numerical efficiency of the MCTDH algorithm. The propagation is then carried out by integration of a set of coupled equations of motion derived from the Dirac-Frenkel variational principle.

The State-averaged Multiconfigurational Time-dependent Hartree (SA-MCTDH) is a modification of the MCTDH method which represents a set of wave functions using a common SPFs set, which adapts at each time step to provide the best basis for the *average* of the wave functions represented. This means that more SPFs will be needed than if the wave functions were represented independently, but has the advantage that the effort to propagate a set of wave functions is then roughly independent of the number of wave functions in the set. Moreover, overlap operations between these functions are straightforwardly performed

since they do not require projections on the SPF basis. This advantage is exploited to calculate eigenstates of general operators by iterative diagonalization, and it has been effectively used in high dimension systems.<sup>55</sup>

## 2.6 Simulation details

Three kinds of calculation were needed in order to obtain the diffusion rates for either the H<sub>2</sub> or D<sub>2</sub>: 1) calculation of the 5D Hamiltonian eigenstates at a minimum of the PES to compute the reactant partition function, 2) calculation of the thermal flux operator eigenstates with a dividing surface set at a maximum of the PES and, finally, 3) the propagation of the latter for a time long enough to ensure convergence of the results. In order to be able to span a large temperature range, the thermal flux eigenstates were calculated and propagated for three different reference temperatures, namely 75, 100, and 150 K, so a total of 7 calculations were carried out on each PES. The wavefunction representation parameters (number of SPFs, primitive functions and grid parameters for each degree of freedom) employed for the calculation and propagation of the thermal flux eigenstates at 150K for the hydrogen molecule using the Ref. 48 PES are found in Table 1. The details regarding the numerical convergence and the basis used for the remaining calculations are given in the Supporting Information. Note that the primitive grid is maintained in all sets of thermal flux eigenstates calculation and propagation, but the number of SPFs changes. This is particularly noticeable in the  $z$  coordinate, associated to the diffusion motion. A Complex Absorbing Potential (CAP) was placed at both edges of the  $z$  coordinate grid, with a length of 9 bohr, to avoid aliasing during the propagation step.

It is worthwhile pointing out that the grid on the  $z$  coordinate is large. This is done in order to allow a good description of the dynamics before the wave packet is absorbed by the CAP. This differs from the work in Ref. 41, where the CAP was placed just in the first minimum after the dividing surface, thus making an *uncorrelated hopping* approximation somewhat equivalent to a classical TST.

**Table 1: Quantum Dynamics of H<sub>2</sub> confined in a (8,0) SWCNT at 150 K and using the Ref. 48 PES: Basis set and grid MCTDH representation for the calculation of thermal flux eigenstates and time propagation.**

DOF	Number of SPFs		Num. Points	Primitive grid	
	Eigenstates	Propagation		Type	Range
$\rho$	2	2	32	FFT	0.5–5.0 $a_0$
$\theta$	5	5	64	cot-DVR	0– $\pi/2$
$\phi$	7	7	64	FFT	0– $2\pi$
$x$	3	4	32	FFT	-3.5–3.5 $a_0$
$y$	3	4	32	FFT	-3.5–3.5 $a_0$
$z$	2	6	256	FFT	-28.033–28.033 $a_0$

### 3 Results and discussion

The calculation of the 50 eigenstates for the H<sub>2</sub> molecule, using the Ref. 48 PES at a reference temperature of 150 K, required 10 h of calculation in a 32-core Intel(R) Xeon(R) E5-4620 0 @ 2.20GHz processor, while 9 h were needed for D<sub>2</sub> under the same conditions. With this number of eigenstates, the last (50<sup>th</sup>) eigenvalue was, in all cases, at most 5 orders of magnitude smaller than the first one. This guarantees that all relevant flux contributions were taken into account for the calculation of  $N(E)$ . The subsequent propagation of these flux eigenstates for 500 fs took 105 h for H<sub>2</sub> and 76 h for D<sub>2</sub> in the same machine for a reference temperature of 150 K. Similar times were required for the calculation carried out under the remaining reference temperatures and with the FB PES.

For the sake of clarity, we focus the following discussion on the results obtained using the Ref. 48 PES. The detailed results corresponding to the FB PES can be found in the Supporting Information, and here only the final diffusion coefficients and selectivities will be discussed.

The flux-position correlation function obtained for the H<sub>2</sub> diffusion simulation at T=150 K is shown in Figure 2. Note that a plateau is reached at  $\sim 200$  fs, although a small decrease can be observed after 300 fs. This could be due to recrossing effects at very large times, but nevertheless we consider that the function is smooth enough to obtain relevant information. On the other hand,  $C_{fp}$  for the deuterium molecule in the same conditions is shown in Fig-

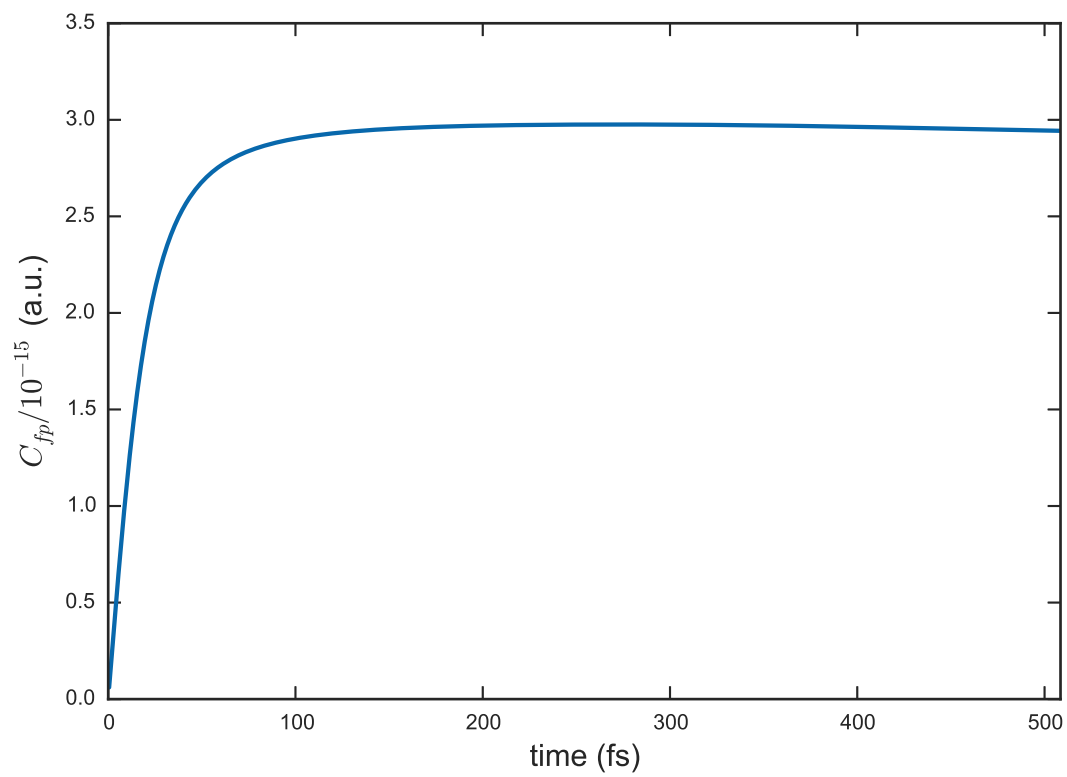


Figure 2: Total flux-position correlation function for the diffusion of H<sub>2</sub> along an (8,0) carbon nanotube at T=150 K, using the Ref. 48 PES.

ure 3. Note the difference in scale between both figures, with the flux-position correlation function for D<sub>2</sub> being three orders of magnitude larger than the one for H<sub>2</sub>. In this case there is no sign of decreasing of the function, which remains flat at  $t > 200$  fs.

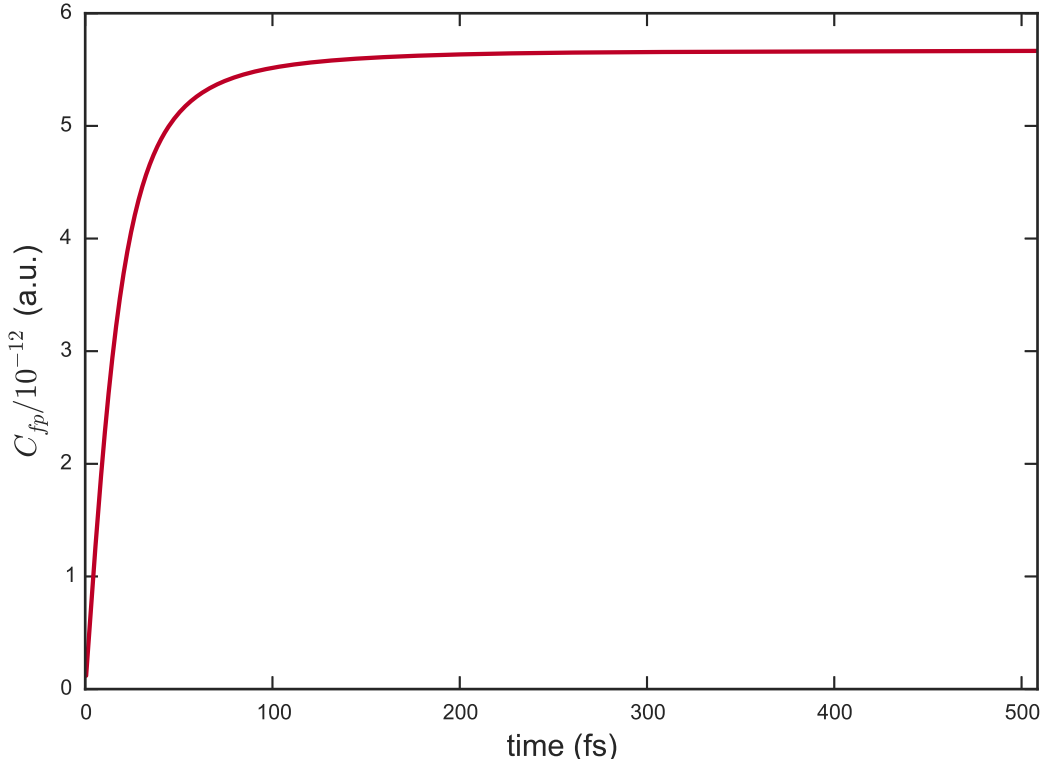


Figure 3: Total flux-position correlation function for the diffusion of D<sub>2</sub> along an (8,0) CNT at T=150 K, using the Ref. 48 PES.

A Fourier transform of the flux-flux correlation function yields the Cumulative Reaction Probability,  $N(E)$ , (see Eq. (7)). This function is plotted as a function of the total energy for the hydrogen and deuterium systems in Figures 4 and 5, respectively. The total cumulative reaction probability, in the darkest color at each figure, increases gradually starting from a certain energy threshold. At first glance a higher energy threshold is identified in the case of H<sub>2</sub> diffusion with respect to D<sub>2</sub>. However, given the low energy barrier (11 cm<sup>-1</sup> in Ref. 48 PES and 37 cm<sup>-1</sup> in FB PES) the different energy threshold observed in the CRP plots can be mainly attributed to the different ZPE of the reactants (2534 cm<sup>-1</sup>  $\sim$  0.31 eV

for  $\text{H}_2$  and  $1820 \text{ cm}^{-1} \sim 0.22 \text{ eV}$  for  $\text{D}_2$  in the Ref. 48 PES). Nevertheless, calculating the adiabatic energy barrier (i.e. considering the ZPE of both reactant and activated complex) reveals that this quantity is slightly higher in the case of  $\text{H}_2$  ( $58 \text{ cm}^{-1}$ ) than in the case of  $\text{D}_2$  ( $45 \text{ cm}^{-1}$ ). This difference in the adiabatic energy barrier can be related to the different vibrational amplitude of both isotopologues' wave function. A smaller vibrational amplitude for  $\text{D}_2$  (lower ZPE), compared to that of  $\text{H}_2$ , results in a less corrugated potential for the heavier molecule as it diffuses along the nanotube. A similar reasoning has been employed by Kumar and Bhatia when studying the quantum confinement effects affecting  $\text{H}_2$  and  $\text{D}_2$  adsorption and diffusion inside a  $\rho$  zeolite.<sup>35</sup>

Another difference between both systems is the rate of increase of  $N(E)$ , which is steeper for  $\text{D}_2$  than for  $\text{H}_2$ . This issue can be explained by decomposing the total CRP into individual probabilities resulting from the flux eigenpairs contributing to the process (25 in this case). In the figures, the individual contribution corresponding to the first five flux eigenstates are depicted together with the CRP, showing the reason for the different pattern between both isotopologues: the density of states participating in deuterium is much larger than in hydrogen, thus explaining the faster increase of the total CRP. The individual contributions oscillate around a probability of  $\sim 1$ , which may be an indication of recrossing effects. It must be pointed out that these contributions are not weighted by the *orto/para* symmetry degeneration numbers. The CRP obtained at the three reference temperature values sampled are essentially the same, as it can be seen in Figures 6 and 7. In these Figures the total  $N(E)$  is shown for the three values of  $\beta$ . Note, however, that the oscillations in the CRP at high energies are more important for the calculation employing a lower reference temperature, which indicates an increasing numerical error. This is the reason why several reference temperatures must be sampled in order to span a larger temperature interval.

The partition functions were initially calculated using both a semiclassical and a quantum approach. The results obtained with both methodologies were not consistent, with differences of several orders of magnitude in their values even at low temperatures. This

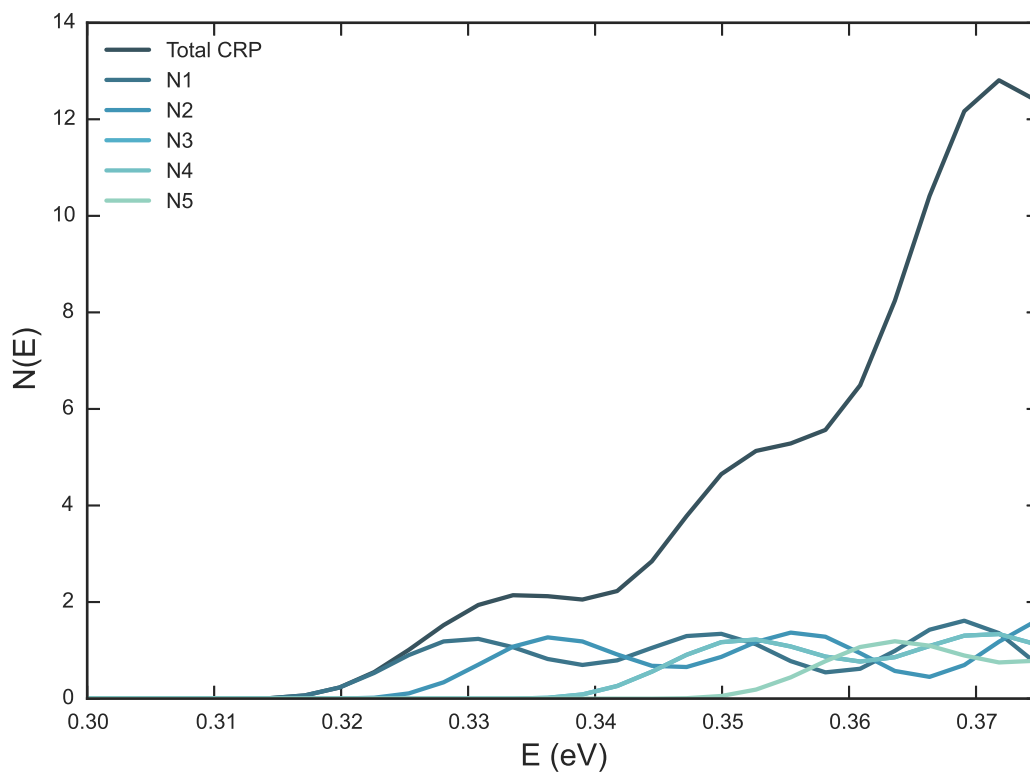


Figure 4: Total (darkest) and the five lower-energy individual reaction probabilities for the diffusion process of  $H_2$  along an (8,0) carbon nanotube at a reference temperature of 150 K, using the Ref. 48 PES. Symmetry numbers due to the rotational parity of  $H_2$  are not taken into account in the curves.

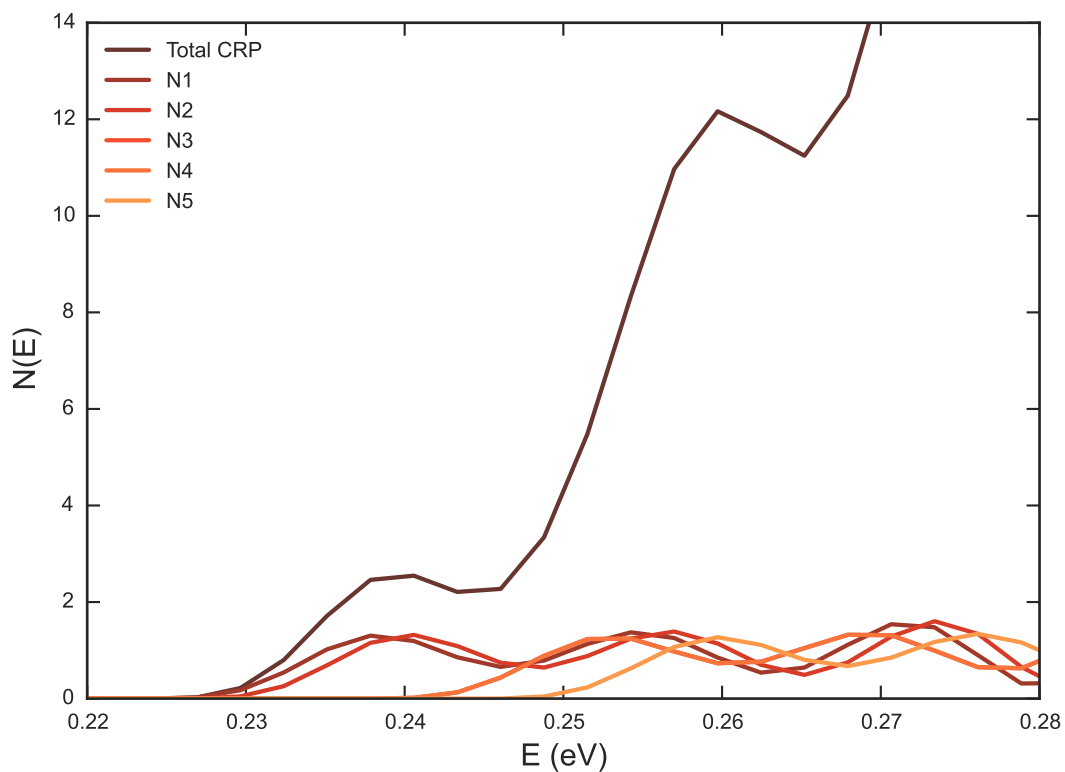


Figure 5: Total (darkest) and the five lower-energy individual probabilities for the process of diffusion of  $D_2$  inside an  $(8,0)$  carbon nanotube at a reference temperature of 150 K, using the Ref. 48 PES. Symmetry numbers due to the rotational parity of  $D_2$  are not taken into account in the curves.

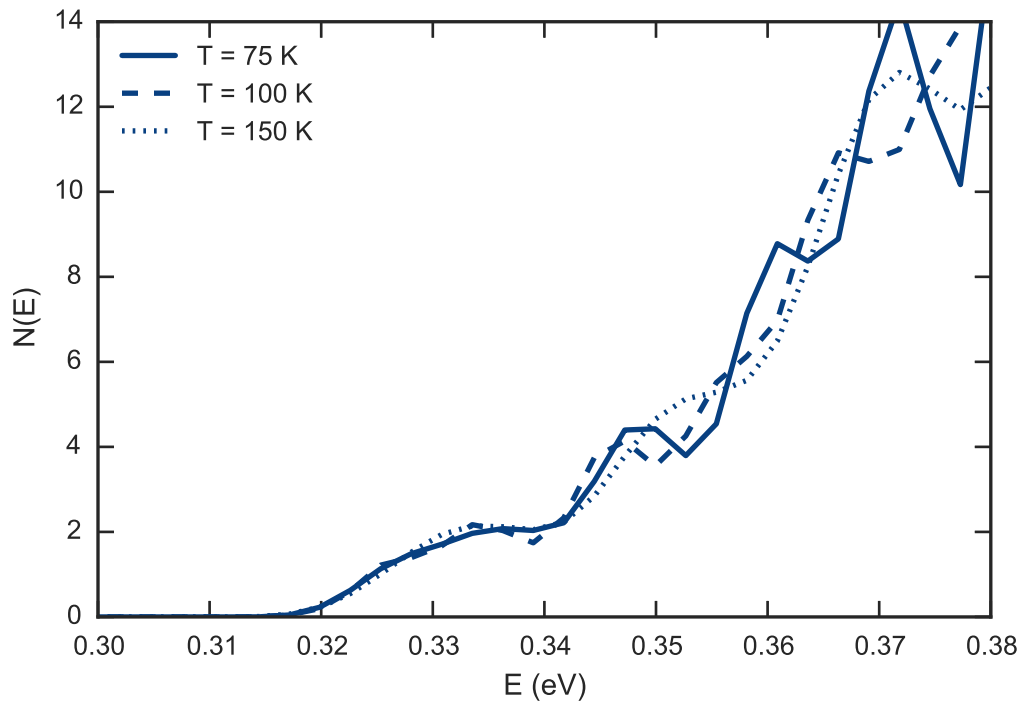


Figure 6: CRP for the  $\text{H}_2@(\text{8},0)$  system at the different temperatures sampled:  $T=75$  K (solid line),  $T=100$  K (dashed line) and  $T=150$  K (dotted line). Symmetry numbers due to the rotational parity of  $\text{H}_2$  are not included.

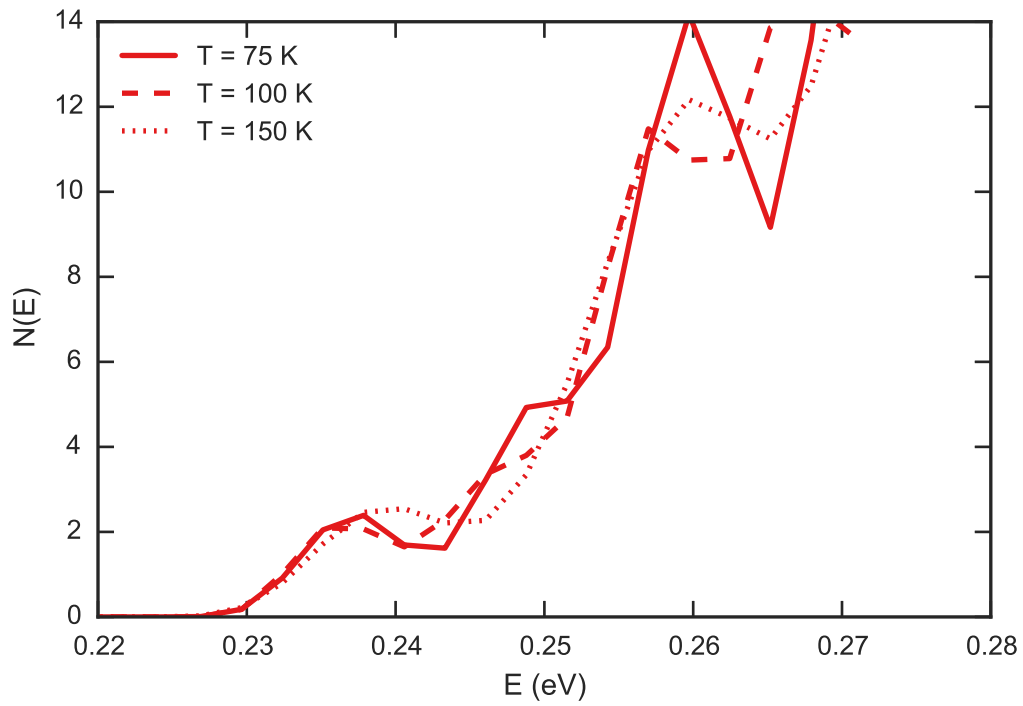


Figure 7: CRP for the  $D_2@(8,0)$  system at the different temperatures sampled:  $T=75$  K (solid line),  $T=100$  K (dashed line) and  $T=150$  K (dotted line). Symmetry numbers due to the rotational parity of  $D_2$  are not included.

fact can be explained by the different ZPE resulting from both approaches: to calculate a semiclassical partition function, one relies on the full separability of the system. Considering this assumption, the total ZPE is the sum of the vibrational ZPE and the ZPE appearing due to the confining potential in  $x$  and  $y$ , which, in our case, is modeled as a harmonic oscillator. However, as it is seen in Figure 1, the potential along  $x$  and  $y$  is significantly anharmonic. In addition to this, as it was reported by one of us,<sup>22</sup> the coupling between the rotational and translational degrees of freedom has a relevant effect on the ZPE of a nanoconfined system. These differences are enough to significantly change the value of the partition function at low temperatures, and for this reason only the results obtained with the quantum approach are shown hereafter.

After thermal averaging the CRP to obtain the hopping probability, diffusion rates are obtained for both H<sub>2</sub> and D<sub>2</sub> according to Eq (1). The results are shown in Fig. 8 as an Arrhenius plot. The data obtained at three reference temperatures using Eqs (7) and (8) is merged in order to span a broader temperature range from 50 to 155 K. No attempt has been made to go below this temperature, since it is expected that intermolecular interactions become increasingly important below this point. Additionally, the same diffusion rates have been calculated using Transition State Theory, obtaining similar results to those calculated by rigorous quantum dynamics. The TST results can be found in the Supporting Information.

Similarly to what has just been discussed, we have computed the corresponding partition functions, CRPs and hopping frequencies for the self-diffusion of H<sub>2</sub> and D<sub>2</sub> along an (8,0) CNT using the FB potential. Detailed results are available in the SI and the final diffusion coefficient values are shown in Fig. 8. Concerning the intermediate data (SI), we would like to mention that there are noticeable differences between the CRPs obtained from both surfaces, presenting a slightly larger energy threshold and a much lower density of states in the case of the FB potential. Nevertheless, the final diffusion rates obtained with both PES are comparable, with a difference of less than an order of magnitude. This seems to imply

that, even though the PES affects the calculation of the CRP and the partition functions, the effects compensate one another, thus providing a similar final result.

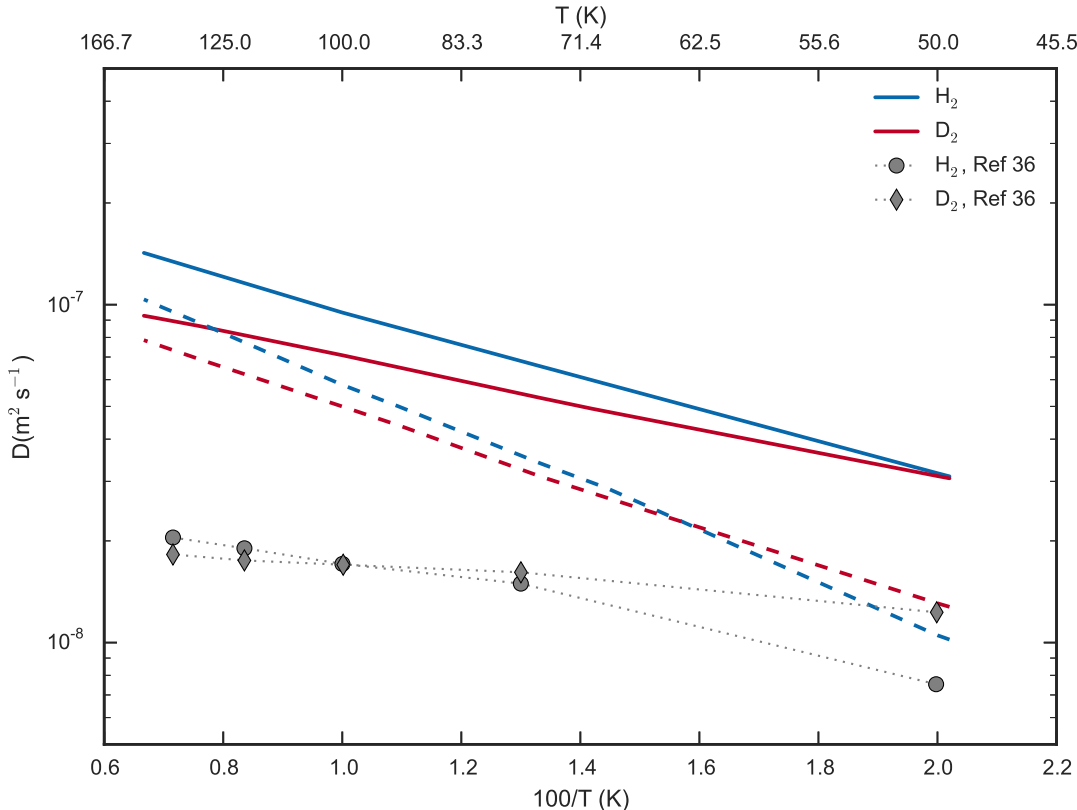


Figure 8: Calculated diffusion rates for hydrogen (blue) and deuterium (red) along an (8,0) carbon nanotube for the Ref. 48 (solid) and FB (dashed) PES. The data obtained using different reference temperatures of 75, 100 and 150 K are combined to span the 50-155 K temperature range. Grey markers correspond to the experimental  $H_2/D_2$  diffusion data in a CMS, extracted from Ref. 36.

The activation energy for the diffusion process is estimated from the slope of the diffusion constant values plotted in Fig 8. The calculated values, shown in Table 2, show that this activation energy is higher for  $H_2$  than for  $D_2$  for both PES studied. This supports our discussion on the reaction probability plots and the corresponding adiabatic energy barriers. As a consequence of this difference in  $E_a$ , a *reverse kinetic isotope effect* appears at low temperatures, *i.e.*, even though at high temperatures  $H_2$  diffuses faster than  $D_2$ , at a certain point in the cold temperature range, this trend is inverted and  $D_2$  starts to diffuse faster than  $H_2$ . This point is located around 50 K for the Ref. 48 PES, and approximately at 62 K

for the FB PES. At the lowest temperature reached by our calculations, deuterium diffusion rate is just slightly larger than hydrogen’s, but the difference is expected to increase at even lower temperatures. In order to illustrate this effect, the ratio of diffusion rates ( $D_{D_2}/D_{H_2}$ ) is plotted in Figure 9 as a function of temperature, for both PESs object of study. This function evidences an increasingly faster  $D_2$  diffusion with respect to  $H_2$  as the temperature is lowered, until for temperatures below 60–50 K the ratio is inverted. The effect is particularly more noticeable in the case of the FB-PES. This trend is consistent with the experimental diffusion rates obtained by Nguyen et al. in a Takeda 3A Carbon Molecular Sieve.<sup>36</sup> The experimental data are shown in Figure 8 only for qualitative comparison purposes. Comparing the results obtained on both Ref. 48 and FB PESs, the larger sieving effects and the higher temperature at which the inversion of the diffusion rates ratio takes place is consistent with the fact that the potential energy barrier is  $\sim 4$  times larger in the FB PES than in the Ref. 48. Despite the quantitative differences, the fact that two inherently different systems such as a CMS and a SWCNT present such a similar qualitative behavior regarding the diffusion of  $H_2$  and  $D_2$  is promising for the development of new molecular sieves taking advantage of the kinetic separation.

**Table 2: Activation energies, in  $\text{cm}^{-1}$ , for the diffusion of  $H_2$  and  $D_2$  inside an (8,0) CNT for the two PES employed.**

	Ref. 48 PES	FB PES
$H_2$	77	107
$D_2$	60	94

At this point it is interesting to consider again the selective adsorption mentioned in the introduction. The quantum sieving effect between isotopologues has been traditionally related with the selective adsorption of the heavier species ( $D_2$ ) over the lighter ( $H_2$ ) due to the difference in ZPE for both species.<sup>17,23,38</sup> This magnitude is represented by the selectivity factor,  $S_0$ , defined as a ratio of equilibrium constants for the adsorption process of both

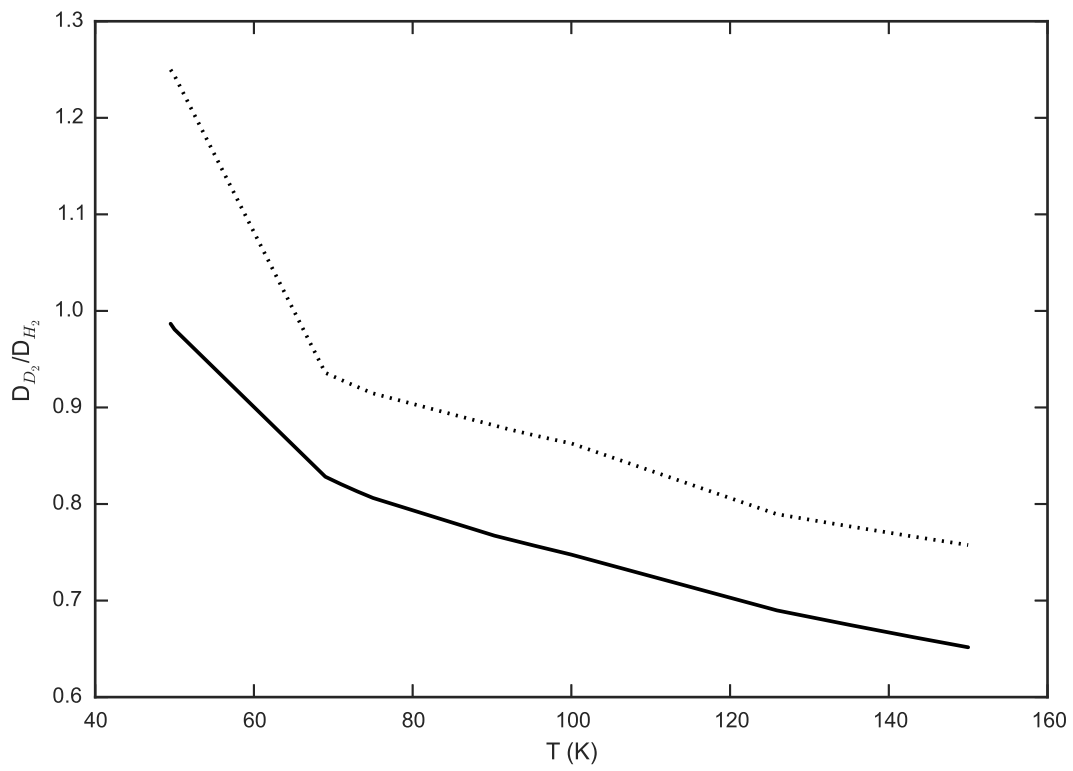


Figure 9: Ratio between the diffusion rates of  $D_2$  and  $H_2$  inside an (8,0) carbon nanotube calculated using the Ref. 48 PES (solid line) and the FB PES (dotted line).

species implicated:

$$S_0(2/1) = \frac{K_2}{K_1} = \frac{Q_{ads,2}Q_{free,1}}{Q_{ads,1}Q_{free,2}}. \tag{15}$$

We have calculated this quantity using our partition functions as explained before. The resulting selectivity factor is shown in Figure 10 for the both Ref. 48 (top panel) and FB PESs (bottom panel). The latter is compared with the results from Ref. 23 on the same PES. Note that there is a significant difference between both PES, the FB-PES predicting a larger adsorption selectivity. This finding was also reported by Garberoglio et al. in Ref. 38. Focusing on the FB potential, our  $S_0$  is in good agreement with the one reported by Lu et al.. The difference at lower temperatures can be related with the different Hamiltonian model used: while they considered a 4D Hamiltonian, freezing the internuclear distance, we treat all DOFs, thus allowing all couplings to appear. Additionally, the slightly different structure of our optimized nanotube with respect to the one used in previous works may lead to subtle changes in the global PES, further explaining the differences between our calculations.

## 4 Summary and conclusions

In the present work we have calculated the diffusion constant for two isotopologues of molecular hydrogen ( $H_2$  and  $D_2$ ) inside a SWCNT using, for the first time, full-dimensional quantum dynamics methods within the single hopping and rigid structure approximations. Two different sets of LJ parameters have been used to model the H-C interaction potential. The diffusion constants obtained by quantum dynamics are similar regardless of the PES used, even though the electronic barriers for diffusion differ by a factor of 4. The general trend is a faster self-diffusion of  $H_2$  in front of  $D_2$  at high temperatures, with this tendency being inverted below 60 K. This difference can be explained in terms of the activation energy, which is higher for hydrogen, in part due to its larger effective size resulting from a higher ZPE.

It is also found that the computed diffusion rates qualitatively agree with experimental

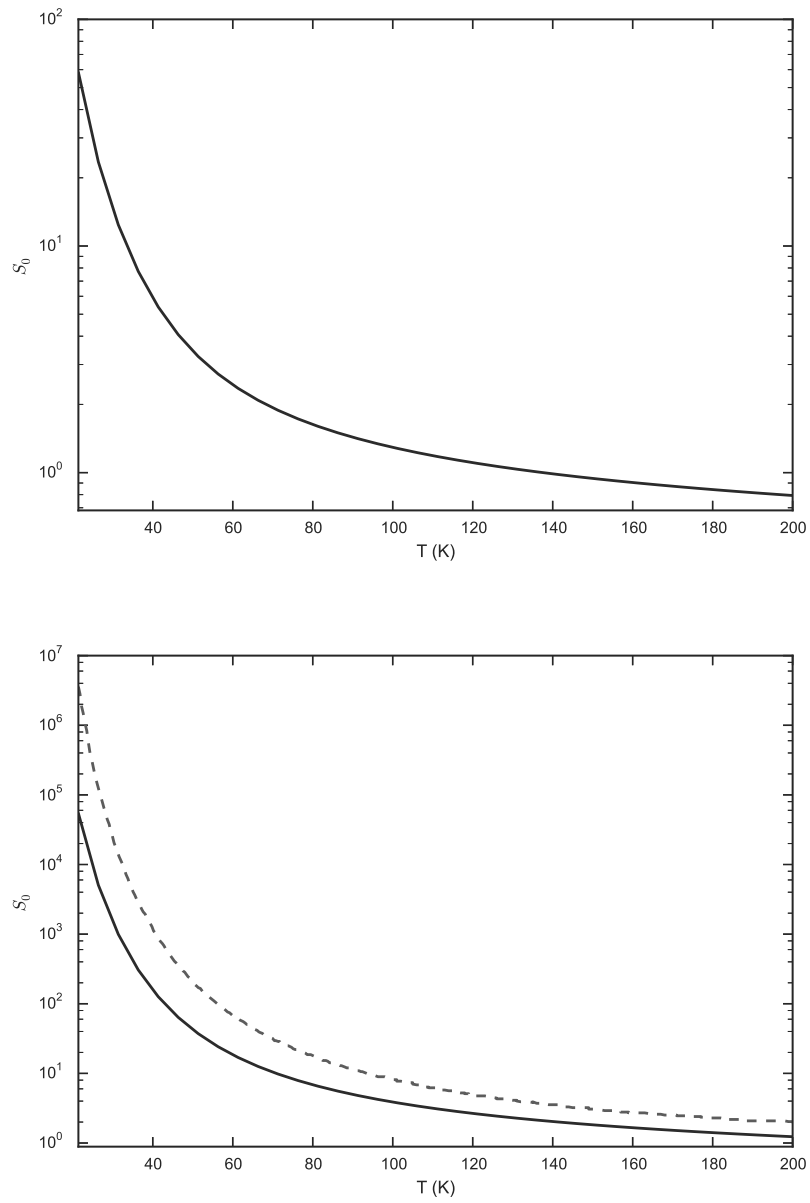


Figure 10: Selectivity factor,  $S_0$ , as a function of temperature for the Ref. 48 (upper panel) and the FB (lower panel) PES. The latter coincides greatly with the one obtained by Lu et al.<sup>23</sup> (dashed line).

results obtained in carbon molecular sieves,<sup>36</sup> even though CMS and CNTs are not strictly comparable systems due to their different structures. The FB PES gives results more similar to experimental data obtained in similar nanostructured materials, which suggests that this potential parameters might be more reliable. We do reproduce previously reported quantum sieving effects in the selectivity factor,  $S_0$ , showing a preferred adsorption of  $D_2$  with respect to  $H_2$ .

The full quantum dynamics formalism used here provides reliable results and gives insight of the diffusion process of light molecules and its isotopologues with valuable detail. Investigation should be now focused on the improvement of the interaction model between the nanotube and the confined molecule, in order to see further effects.

## Acknowledgement

Financial support from the Spanish Ministerio de Economía y Competitividad (Ministry of Economy and Competitiveness) (CTQ2013-41307-P) and Generalitat de Catalunya (2014-SGR-25) is acknowledged. M.M.-M. further thanks a predoctoral grant from the FPU program (FPU2013/02210) from the Spanish Ministerio de Educación, Cultura y Deporte (Ministry of Education, Culture and Sports). The authors thank Prof. Uwe Manthe for his advice in the design of the propagations, and the reviewers for pointing out some inconsistencies in our first calculations.

## Supporting Information Available

Numerical details regarding the convergence of the different sets of calculations performed. Intermediate results obtained for the Frankland–Brenner potential. Final results obtained by Transition State Theory.

This material is available free of charge via the Internet at <http://pubs.acs.org/>.

## References

- (1) Ioannatos, G. E.; Verykios, X. E. H<sub>2</sub> Storage on Single- and Multi-Walled Carbon Nanotubes. *Int. J. Hydrogen Energy* **2010**, *35*, 622–628.
- (2) Ren, X.; Chen, C.; Nagatsu, M.; Wang, X. Carbon Nanotubes as Adsorbents in Environmental Pollution Management: A Review. *Chem. Eng. J.* **2011**, *170*, 395–410.
- (3) Gibson, R. F.; Ayorinde, E. O.; Wen, Y.-F. Vibrations of Carbon Nanotubes and their Composites: A Review. *Compos. Sci. Technol.* **2007**, *67*, 1–28.
- (4) Santamaría-Holek, I.; Reguera, D.; Rubi, J. M. Carbon-Nanotube- Based Motor Driven by a Thermal Gradient. *J. Phys. Chem. C* **2013**, *117*, 3109–3113.
- (5) Jain, P. K.; Huang, X.; El-Sayed, I. H.; El-Sayed, M. A. Noble Metals on the Nanoscale: Optical and Photothermal Properties and Some Applications in Imaging, Sensing, Biology, and Medicine. *Acc. Chem. Res.* **2008**, *41*, 1578–1586.
- (6) Aricò, A. S.; Bruce, P.; Scrosati, B.; Tarascon, J.-M.; van Schalkwijk, W. Nanostructured Materials for Advanced Energy Conversion and Storage Devices. *Nature Materials* **2005**, *4*, 366–377.
- (7) Wang, J. Carbon-nanotube Based Electrochemical Biosensors: A Review. *Electroanalysis* **2005**, *17*, 7–14.
- (8) Eijkel, J. C. T.; van den Berg, A. Nanofluidics: What Is It and What Can We Expect from It? *Microfluid. Nanofluidics* **2005**, *1*, 249–267.
- (9) Millward, A. R.; Yaghi, O. M. Metal-Organic Frameworks with Exceptionally High Capacity for Storage of Carbon Dioxide at Room Temperature. *J. Am. Chem. Soc.* **2005**, *127*, 17998–9.

- (10) Todd, A. C.; Tohidi, B.; Fredheim, A.; Maitland, G.; Fennell, P.; Brandani, S.; Gibbins, J.; Stevens, G.; Fatemi, S.; Vesali-Naseh, M. et al. Improving CO<sub>2</sub>/CH<sub>4</sub> Adsorptive Selectivity of Carbon Nanotubes by Functionalization with Nitrogen-Containing Groups. *Chem. Eng. Res. Des.* **2011**, *89*, 1669–1675.
- (11) Schlapbach, L.; Züttel, A. Hydrogen-Storage Materials for Mobile Applications. *Nature* **2001**, *414*, 353–358.
- (12) Cheng, H.-M.; Yang, Q.-H.; Liu, C. Hydrogen Storage in Carbon Nanotubes. *Carbon* **2001**, *39*, 1447–1454.
- (13) Morris, R. E.; Wheatley, P. S. Gas Storage in Nanoporous Materials. *Angew. Chemie - Int. Ed.* **2008**, *47*, 4966–4981.
- (14) Dillon, A. C.; Jones, K. M.; Bekkedahl, T. A.; Kiang, C. H.; Bethune, D. S.; Heben, M. J. Storage of Hydrogen in Single-Walled Carbon Nanotubes. *Nature* **1997**, *386*, 377–379.
- (15) Atwood, J. L.; Barbour, L. J.; Jerga, A. Storage of Methane and Freon by Interstitial Van der Waals Confinement. *Science (New York, N.Y.)* **2002**, *296*, 2367–2369.
- (16) Mueller, U.; Schubert, M.; Teich, F.; Puetter, H.; Schierle-Arndt, K.; Pastré, J. Metal-Organic Frameworks—Prospective Industrial Applications. *J. Mater. Chem.* **2006**, *16*, 626–636.
- (17) Beenakker, J.; Borman, V.; Krylov, S. Molecular Transport in Subnanometer Pores: Zero-Point Energy, Reduced Dimensionality and Quantum Sieving. *Chem. Phys. Lett.* **1995**, *232*, 379–382.
- (18) Mondelo-Martell, M.; Huarte-Larrañaga, F. 5D Quantum Dynamics of the H<sub>2</sub>@SWNT System: Quantitative Study of the Rotational-Translational Coupling. *J. Chem. Phys.* **2015**, *142*, 084304–15.

- (19) Mondelo-Martell, M.; Huarte-Larrañaga, F. Six Dimensional Propagation of the H<sub>2</sub> Molecule Confined in a Single-Walled Carbon Nanotube. *Chem. Phys.* **2015**, *462*, 41–50.
- (20) Xu, M.; Ye, S.; Lawler, R.; Turro, N. J.; Bačić, Z. HD In C<sub>60</sub>: Theoretical Prediction of the Inelastic Neutron Scattering Spectrum and its Temperature Dependence. *Philos. Trans. A. Math. Phys. Eng. Sci. Mathematical*, **2013**, *371*, 20110630–15.
- (21) Matanović, I.; Belof, J. L.; Space, B.; Sillar, K.; Sauer, J.; Eckert, J.; Bačić, Z. Hydrogen Adsorbed in a Metal Organic Framework-5: Coupled Translation-Rotation Eigenstates from Quantum Five-Dimensional Calculations. *J. Chem. Phys.* **2012**, *137*, 14701–13.
- (22) Suarez, J.; Huarte-Larranaga, F. Hydrogen Confined in Single-Wall Carbon Nanotubes: Anisotropy Effects on Ro-Vibrational Quantum Levels. *J. Chem. Phys.* **2012**, *137*, 064320–13.
- (23) Lu, T.; Goldfield, E. E. M.; Gray, S. S. K. Quantum States of Hydrogen and its Isotopes Confined in Single-Walled Carbon Nanotubes: Dependence on Interaction Potential and Extreme Two-Dimensional Confinement. *J. Phys. Chem. B* **2006**, *110*, 1742–1751.
- (24) Yildirim, T.; Harris, A. Quantum Dynamics of a Hydrogen Molecule Confined in a Cylindrical Potential. *Phys. Rev. B* **2003**, *67*, 245413–15.
- (25) Yim, W.-L.; Byl, O.; Yates, J. T.; Johnson, J. K. Vibrational Behavior of Adsorbed CO<sub>2</sub> on Single-Walled Carbon Nanotubes. *J. Chem. Phys.* **2004**, *120*, 5377–5386.
- (26) Valdés, Á.; Arismendi-Arrieta, D. J.; Prosmiiti, R. Quantum Dynamics of Carbon Dioxide Encapsulated in the Cages of the Si Clathrate Hydrate: Structural Guest Distributions and Cage Occupation. *J. Phys. Chem. C* **2015**, *119*, 3945–3956.
- (27) Wang, Q.; Challa, S.; Sholl, D.; Johnson, J. Quantum Sieving in Carbon Nanotubes and Zeolites. *Phys. Rev. Lett.* **1999**, *82*, 956–959.

- (28) Hankel, M.; Zhang, H.; Nguyen, T. X.; Bhatia, S. K.; Gray, S. K.; Smith, S. C. Kinetic Modelling of Molecular Hydrogen Transport in Microporous Carbon Materials. *Phys. Chem. Chem. Phys.* **2011**, *13*, 7834–44.
- (29) Inokuma, Y.; Kawano, M.; Fujita, M. Crystalline Molecular Flasks. *Nature Chemistry* **2011**, *3*, 349–358.
- (30) Nielsen, T. K.; Bösenberg, U.; Gosalawit, R.; Dornheim, M.; Cerenius, Y.; Besenbacher, F.; Jensen, T. R. A Reversible Nanoconfined Chemical Reaction. *ACS nano* **2010**, *4*, 3903–3908.
- (31) Martinez de la Hoz, J. M.; Balbuena, P. B. Small-Molecule Activation Driven by Confinement Effects. *ACS Catal.* **2015**, *5*, 215–224.
- (32) Kumar, A. V. A.; Jobic, H.; Bhatia, S. K. Quantum Effects on Adsorption and Diffusion of Hydrogen and Deuterium in Microporous Materials. *J. Phys. Chem. B* **2006**, *110*, 16666–71.
- (33) Garberoglio, G. Quantum Sieving in Organic Frameworks. *Chem. Phys. Lett.* **2009**, *467*, 270–275.
- (34) Skouteris, D.; Laganà, A. MCTDH Calculations on the Rigid OH Radical Moving Along a (10,0) Carbon Nanotube. *Chem. Phys. Lett.* **2013**, *575*, 18–22.
- (35) Kumar, A. V. A.; Bhatia, S. K. Quantum Effect Induced Reverse Kinetic Molecular Sieving in Microporous Materials. *Phys. Rev. Lett.* **2005**, *95*, 1–4.
- (36) Nguyen, T. X.; Jobic, H.; Bhatia, S. K. Microscopic Observation of Kinetic Molecular Sieving of Hydrogen Isotopes in a Nanoporous Material. *Phy. Rev. Lett.* **2010**, *105*, 085901.
- (37) Contescu, C. I.; Zhang, H.; Olsen, R. J.; Mamontov, E.; Morris, J. R.; Gallego, N. C.

- Isotope Effect on Adsorbed Quantum Phases: Diffusion of H<sub>2</sub> and D<sub>2</sub> in Nanoporous Carbon. *Phys. Rev. Lett.* **2013**, *110*, 236102–5.
- (38) Garberoglio, G.; DeKlavon, M. M.; Johnson, J. K. Quantum Sieving in Single-Walled Carbon Nanotubes: Effect of Interaction Potential and Rotational-Translational Coupling. *J. Phys. Chem.. B* **2006**, *110*, 1733–1741.
- (39) Pouthier, V.; Light, J. C. Surface Self-Diffusion of Hydrogen on Cu(100): A Quantum Kinetic Equation Approach. *J. Chem. Phys.* **2000**, *113*, 1204–1216.
- (40) Firmino, T.; Marquardt, R.; Gatti, F.; Dong, W. Diffusion Rates for Hydrogen on Pd(111) from Molecular Quantum Dynamics Calculations. *J. Phys. Chem. Lett.* **2014**, *5*, 4270–4274.
- (41) Zhang, D. H.; Light, J. C.; Lee, S.-Y. Y. Transition State Wave Packet Study of Hydrogen Diffusion on Cu(100) Surface. *J. Chem. Phys.* **1999**, *111*, 5741–5753.
- (42) Jaquet, R.; Miller, W. H. Quantum Mechanical Rate Constants Via Path Integrals: Diffusion of Hydrogen Atoms on a Tungsten(100) Surface. *J. Phys. Chem.* **1985**, *89*, 2139–2144.
- (43) Doll, J. D.; Voter, A. F. Recent Developments in the Theory of Surface Diffusion. *Annu. Rev. Phys. Chem.* **1987**, *38*, 413–431.
- (44) Barth, J. Transport of Adsorbates at Metal Surfaces: From Thermal Migration to Hot Precursors. *Surf. Sci. Rep.* **2000**, *40*, 75–149.
- (45) Zhang, D. H.; Light, J. C. Cumulative Reaction Probability Via Transition State Wave Packets. *J. Chem. Phys.* **1996**, *104*, 6184–6191.
- (46) Miller, W. H. Quantum Mechanical Transition State Theory and a New Semiclassical Model for Reaction Rate Constants. *J. Chem. Phys.* **1974**, *61*, 1823–1834.

- (47) Dovesi, R.; Orlando, R.; Civalieri, B.; Roetti, C.; Saunders, V. R.; Zicovich-Wilson, C. M.; Pascale, F.; Doll, K.; Harrison, N. M.; Bush, I. J. et al. Crystal 09 User's Manual. 2009.
- (48) Huarte-Larrañaga, F.; Albertí, M. A Molecular Dynamics Study of the Distribution of Molecular Hydrogen Physisorbed on Single Walled Carbon Nanotubes. *Chem. Phys. Lett.* **2007**, *445*, 227–232.
- (49) Huarte-Larrañaga, F.; Manthe, U. Thermal Rate Constants for Polyatomic Reactions: First Principles Quantum Theory. *Zeitschrift für Phys. Chemie* **2007**, *221*, 171–213.
- (50) Miller, W. H.; Schwartz, S. D.; Tromp, J. W. Quantum Mechanical Rate Constants for Bimolecular Reactions. *J. Chem. Phys.* **1983**, *79*, 4889–4898.
- (51) Matzkies, F.; Manthe, U. Accurate Quantum Calculations of Thermal Rate Constants Employing MCTDH:  $\text{H}_2 + \text{OH} \rightarrow \text{H} + \text{H}_2\text{O}$  and  $\text{D}_2 + \text{OH} \rightarrow \text{D} + \text{DOH}$ . *J. Chem. Phys.* **1998**, *108*, 4828–4836.
- (52) Manthe, U.; Matzkies, F. Quantum Calculations of Thermal Rate Constants and Reaction Probabilities:  $\text{H}_2 + \text{CN} \rightarrow \text{H} + \text{HCN}$ . *Chem. Phys. Lett.* **1998**, *282*, 442–449.
- (53) Manthe, U. The State Averaged Multiconfigurational Time-Dependent Hartree Approach: Vibrational State and Reaction Rate Calculations. *J. Chem. Phys.* **2008**, *128*, 64108–12.
- (54) Meyer, H.-D.; Manthe, U.; Cederbaum, L. The Multi-Configurational Time-Dependent Hartree Approach. *Chem. Phys. Lett.* **1990**, *165*, 73–78.
- (55) Hammer, T.; Manthe, U. Iterative Diagonalization in the State-Averaged Multi-Configurational Time-Dependent Hartree Approach: Excited State Tunneling Splittings in Malonaldehyde. *J. Chem. Phys.* **2012**, *136*, 54105–17.

# Graphical TOC Entry

